MUC-NOTE-COOL_THEORY-296
Revised 16 August 2004

Front-end design for neutrino factory Study 2a

R.C. Fernow, J.S. Berg, J.C. Gallardo, H.G. Kirk & R.B. Palmer
Brookhaven National Laboratory

D. Neuffer
Fermilab

K. Paul
U. Illinois

9 August 2004

We describe a new front end design for a neutrino factory. This design, denoted as Study 2a, was done as part of the APS study on the physics of neutrinos. The channel is 295 m long and produces 0.17 μ / p into the accelerator transverse acceptance of 30 mm and longitudinal acceptance of 150 mm.

1. Introduction

A detailed design [1] for a front end of a neutrino factory was given in the U.S. Muon Collaboration's second feasibility study (FS2). With a 1 MW proton driver the front end produced 0.17 μ/p into an accelerator transverse acceptance of 15 mm and longitudinal acceptance of 150 mm. However, the front end was very expensive and subsequent simulation R&D was devoted to finding a new configuration that could produce the same number of useable muons at less cost. The idea for the adiabatic buncher was developed as part of this effort [2]. This new concept replaces the induction linacs and fixed frequency RF bunching cavities in FS2 with a string of varying frequency RF cavities. It was also realized that the accelerator transverse acceptance could be increased from 15 to 30 mm for a moderate increase in cost. This allowed a much simpler and shorter cooling channel to be designed, which gave the same number of muons in the new accelerator acceptance. These ideas were incorporated into a new design, which we call Study 2a, as part of the 2004 APS study on the physics of neutrinos [3].

The overall layout of the front end was originally designed by R. Palmer [4]. During the course of Study 2a the design was made more realistic by

- generating the field from a single table of coils
- carefully matching the fields at geometrical boundaries
- studying optimized collection field profiles
- adding a tapered beampipe in the collection region
- adding RF windows in the buncher
- discretizing the RF frequencies
- setting the cooler RF frequency to 201.25 MHz
- adding Be coating over the LiH absorbers
- generating new MARS beam distributions

The final layout is shown schematically in Fig. 1.

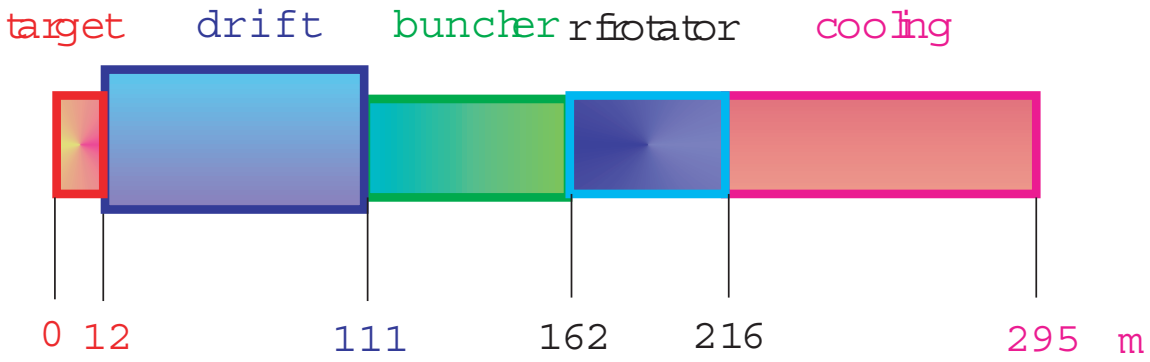

Figure 1. Schematic layout of Study 2a front end.

The first ≈12 m is used to capture pions produced in the target. The field here drops adiabatically from 20 T over the target down to 1.75 T. At the same time, the radial aperture of the beam pipe increases from 7.5 cm at the target up to 25 cm. Next comes ≈100 m for the pions to decay into muons and for the energy-time correlation to develop. The adiabatic bunching occupies the next ≈50 m and the phase rotation ≈50 m following that. Lastly, the channel has ≈80 m of ionization cooling. The total length of the new front end is 295 m.

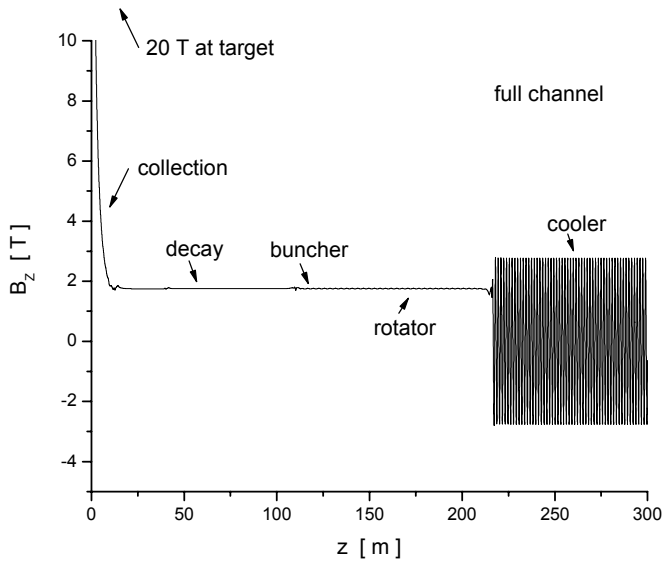

Figure 2. Longitudinal on-axis field for the Study 2a front end.

Focusing in the front end is accomplished by using 460 solenoid coils. The on-axis longitudinal field is shown for the full front-end in Fig. 2. The field falls very rapidly in the collection region to a value of 1.75 T. It keeps this value with very little ripple over the decay, buncher and rotator regions. After a short matching section, the 1.75 T field is changed adiabatically to the alternating field used in the cooler.

2. Target and capture

The target arrangement for Study 2a was identical to that used in FS2. A 24 GeV proton beam was assumed to be incident on a pulsed mercury jet. The interaction takes place inside a 20 T solenoidal field. The jet was incident at an angle of 100 mr to the solenoid axis. The beam was incident at 67 mr to the field axis, giving a 33 mr crossing angle between the beam and the target jet. However, the coils in the vicinity of the target were reconfigured for this study, so new MARS particle production files had to be created. Figure 3 shows that the axial magnetic field peaks at around 20 T in the center of the target and drops off by ~5% at the ends.

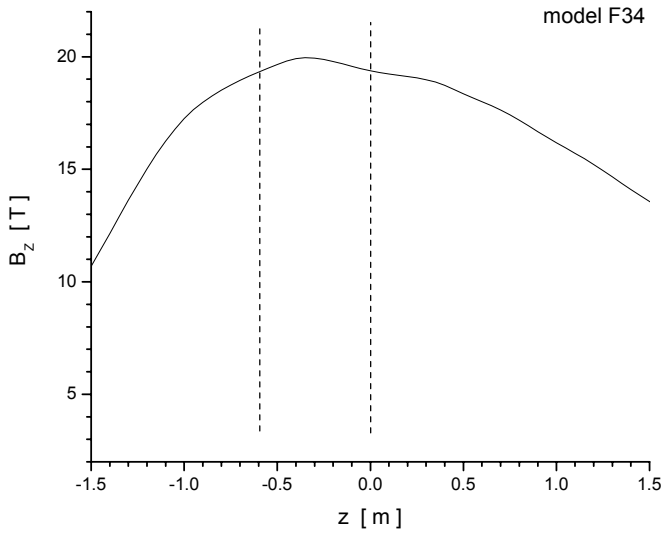

Figure 3. Axial field near the target.[1]

The new MARS production file gave ~8% worse performance than the production file used for FS2. There are strong indications that the performance quoted in FS2 was obtained with a 0^o crossing angle.

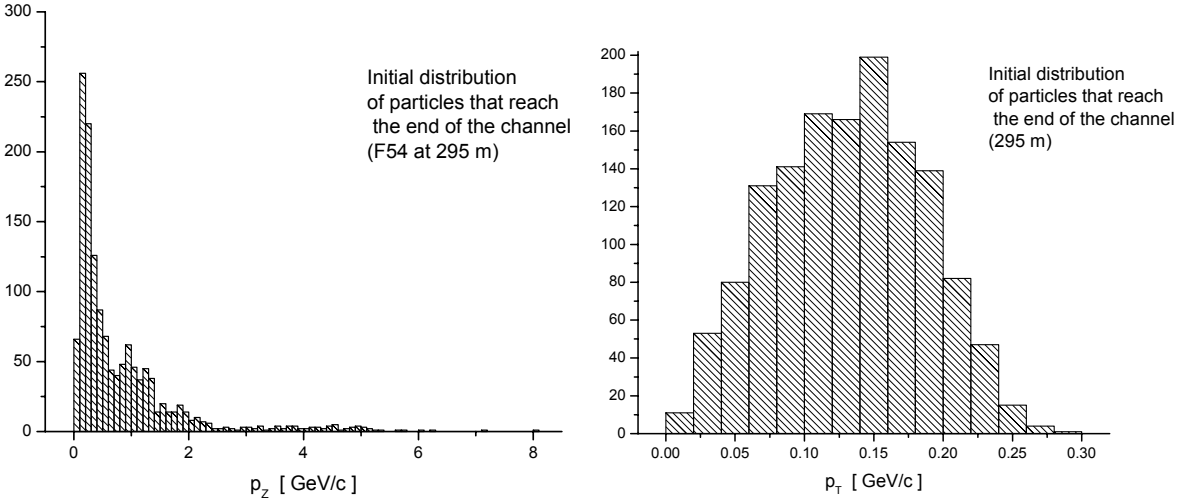

Figure 4. Longitudinal (left) and transverse (right) momentum distributions of particles at the target that are transmitted to the end of the front end channel.

The initial distribution of particles that were propagated to the end of the front-end channel is shown in Fig. 4. The accepted particles have a peak initial longitudinal

[1] In this and subsequent figures the notation F*xx* refers to a private system for identifying simulations.

momentum of ≈200 MeV/c with a long high-energy tail, and a peak initial transverse momentum ≈150 MeV/c.

We used an improved axial field profile in the capture region that increased the final number of muons per proton in the accelerator acceptance by ≈10%. The new axial field profile (marked KP) is compared in Fig. 5 with the profile used in FS2.

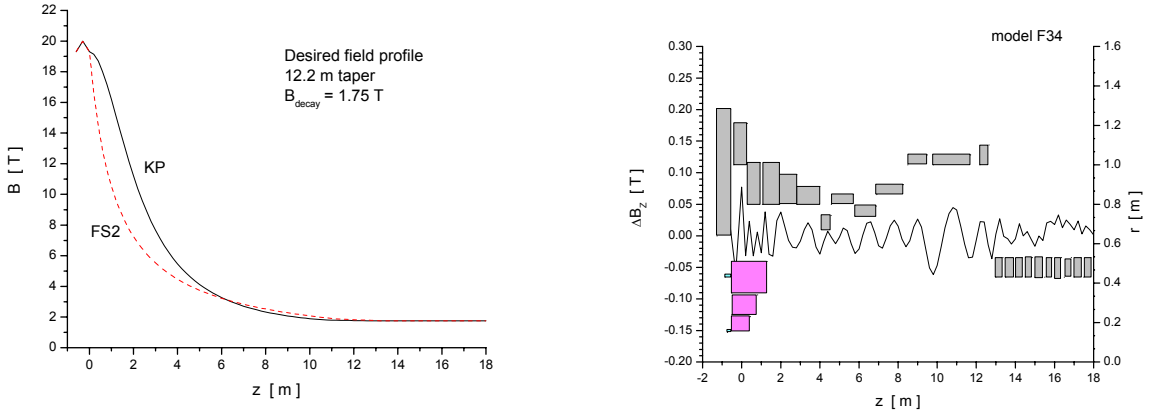

Figure 5. (left) Comparison of the desired axial field profile used here (KP) with the desired profile from Study 2 (FS2); (right) actual coil configuration used to produce the desired field profile.

Figure 5 also shows the actual coil configuration in the collection region. The end of the 60 cm long target region is defined as z = 0. The three small radius coils near z = 0 are Cu coils, while the others are superconducting. The left axis shows the error field on-axis compared with the desired field profile. We see that the peak error field is ≈ 0.07 T.

Figure 6 shows a MARS calculation of the absorbed radiation dose in the collection region.

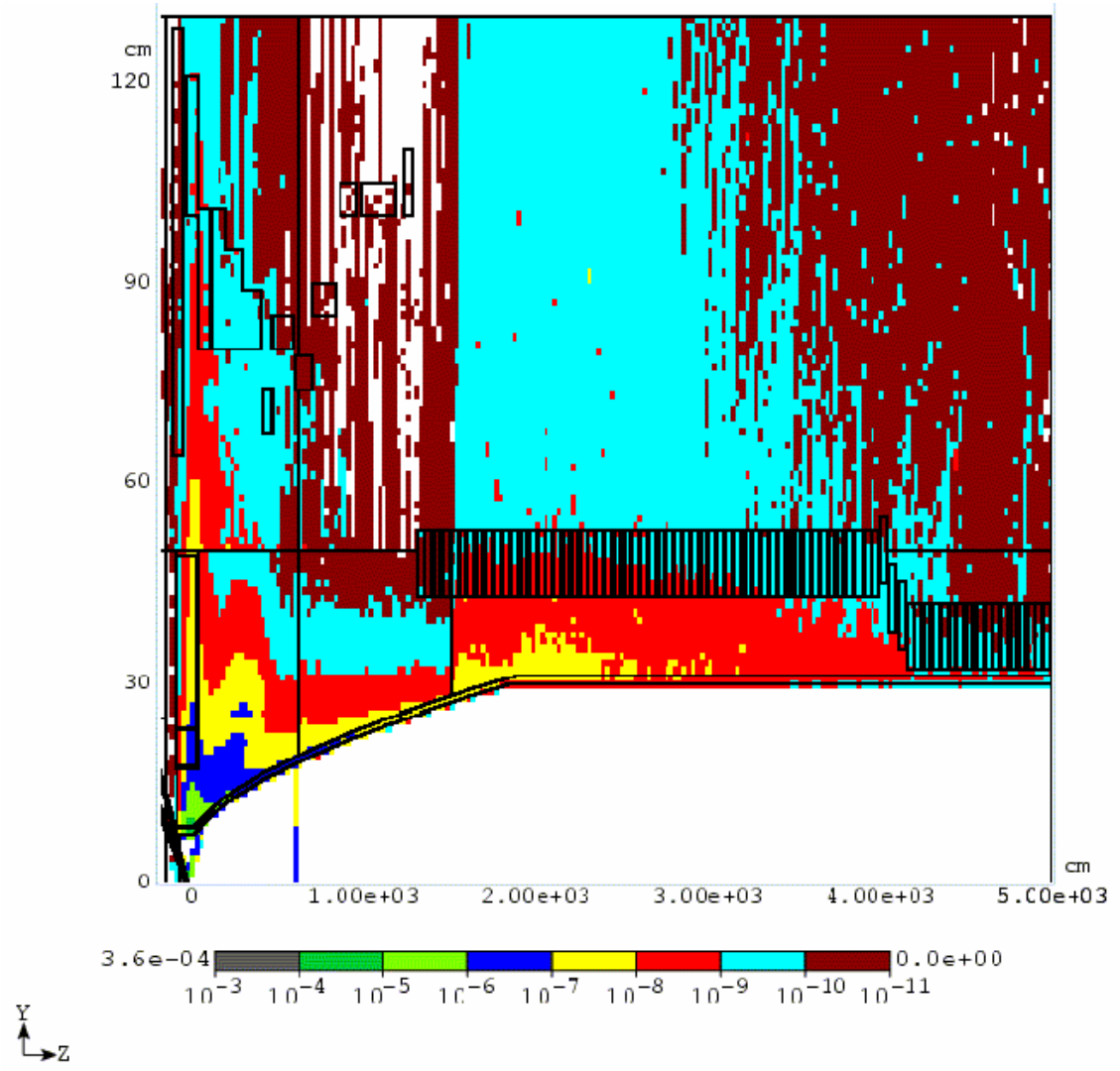

Figure 6. MARS calculation of the absorbed radiation dose in the collection region.

The peak deposition in the superconducting coils is ≈ 1 Mgy/yr for a 1 MW beam running for 1 Snowmass year of 10^7 s. Assuming a lifetime dose for the insulation of 100 Mgy, there should be no problem with radiation damage in the coils.

3. Bunching and phase rotation

A cell of the buncher lattice is shown schematically in Fig. 7. Most of the 75 cm cell length is occupied by the 50-cm-long RF cavity. The cavity iris is covered with a Be window. The limiting radial aperture in the cell is determined by the 25 cm radius of the window. The window thickness varied from 200 – 395 μm.

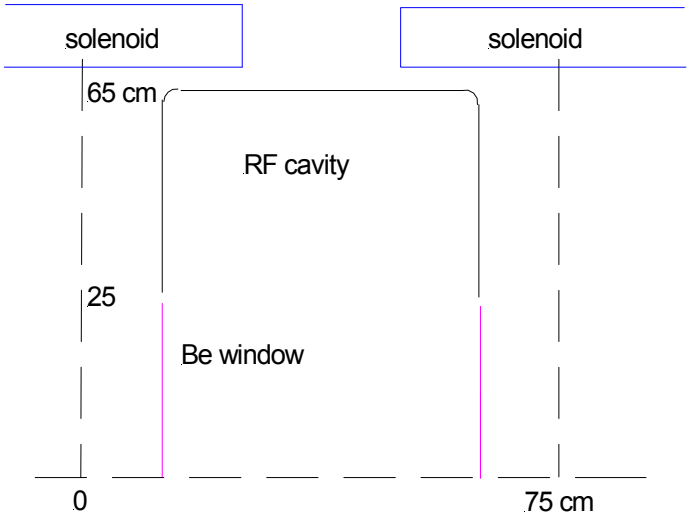

Figure 7. One cell of the buncher lattice.

The 50-cm-long solenoid was placed outside the RF cavity in order to decrease the magnetic field ripple on the axis and minimize beam losses from momentum stop bands. The buncher section contains 27 cavities with 13 discrete frequencies and gradients varying from 5–10 MV/m. The frequencies decrease from 333 to 234 MHz in the buncher region. The cavities are not equally spaced.

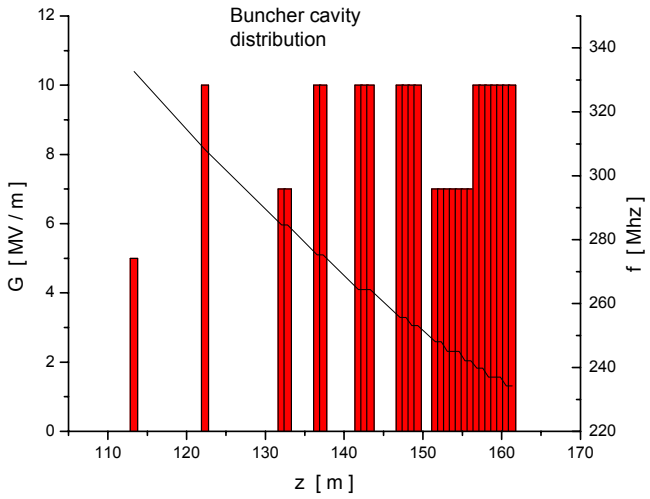

Figure 8. Distribution of cavities in the buncher; gradient (left scale) and frequency (right scale).

Figure 8 shows the distribution of RF cavities in the buncher. Fewer cavities are used at the beginning where the required gradients are small. The rectangles indicate the cavity's longitudinal position. The height of the rectangle gives the cavity gradient, while the continuous curve gives the frequency.

Longitudinal phase space distributions are shown in Fig. 9 after the drift space (left) and after the buncher (right).

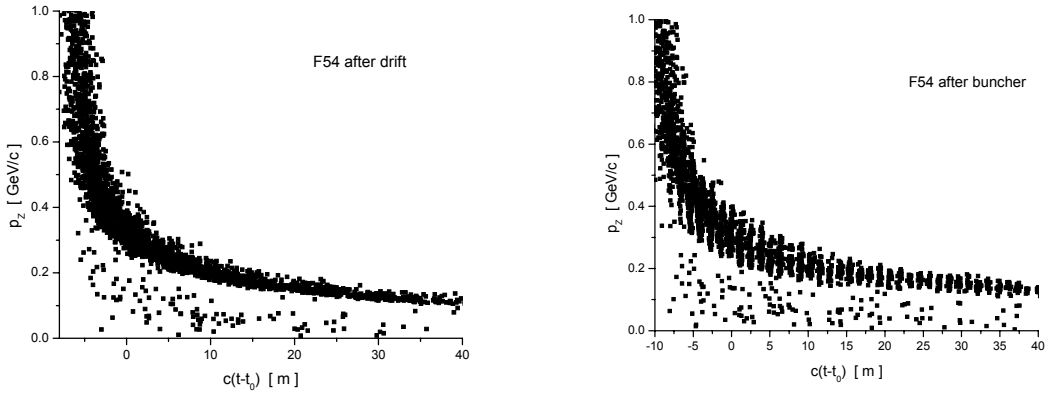

Figure 9. Longitudinal phase distribution after the drift space (left) and after the buncher (right).

The rotator cell is very similar to the buncher cell. The major difference is the use of tapered Be windows on the cavities because of the higher RF gradient. The window thickness was 750 μm out to 20 cm, and 1500 μm from 20 to 25 cm. One cell of the rotator lattice is shown in Fig. 10.

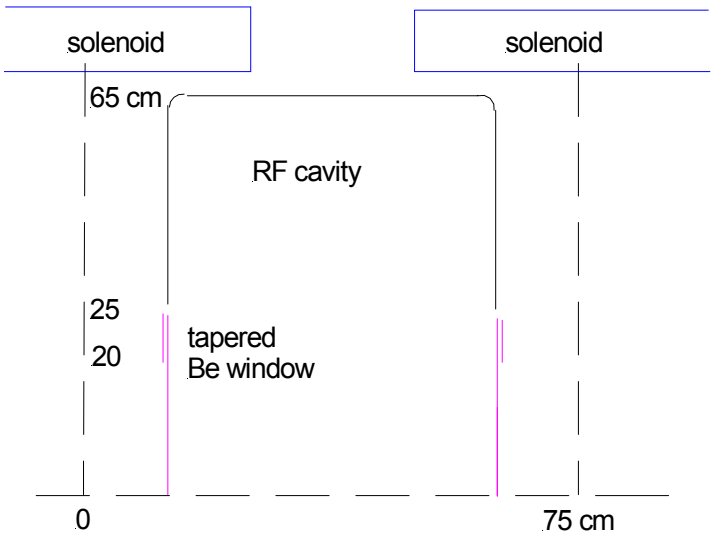

Figure 10. One cell of the rotator lattice.

There are 72 cavities in the rotator region, with 15 different frequencies. The frequencies decrease from 232 to 201 MHz in this part of the front end. All cavities have a gradient of 12.5 MV/m. The energy spread in the beam is significantly reduced, as shown in Fig. 11.

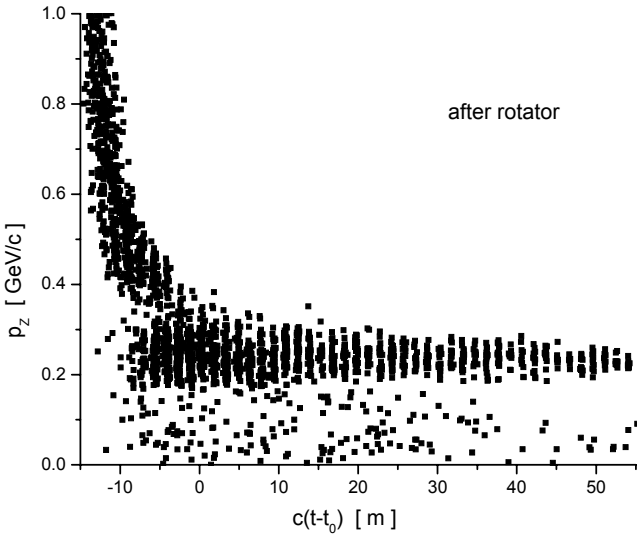

Figure 11. Longitudinal phase space after the rotator.

4. Cooling

Much of the cost savings in the present study comes from the simplified cooling lattice. One half-cell of the channel is shown in Fig. 12.

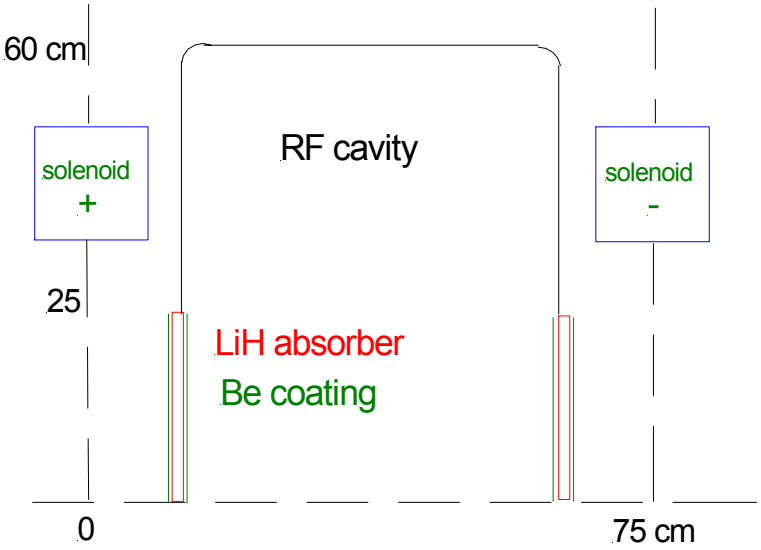

Figure 12. One half-cell of the cooling lattice.

The cooling channel was designed to have a relatively flat transverse beta function with a magnitude of about 80 cm, as seen in Fig. 13.

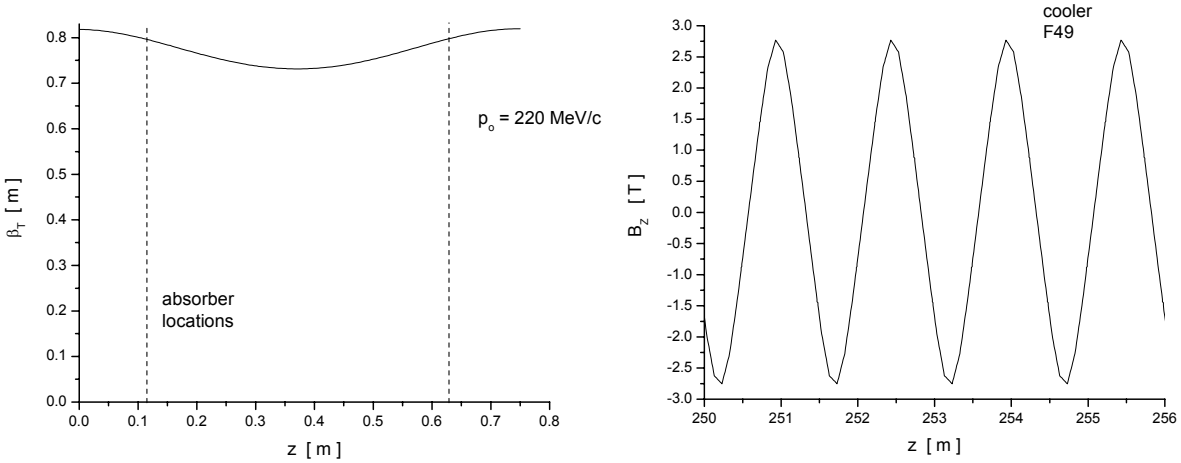

Figure 13. (left) Beta function in one half-cell of the cooling lattice; (right) corresponding longitudinal magnetic field.

The corresponding longitudinal magnetic field in the lattice is also shown. Most of the 150 cm cell length is taken up by the 50-cm-long rf cavities. The cavities have a frequency of 201.25 MHz and a gradient of 15.25 MV/m. A novel aspect of this design comes from using the windows on the RF cavity as the cooling absorbers. This is possible because the near constant β function does not significantly increase the emittance heating at the window location. The window consists of a 1 cm thickness of LiH with 25 μm thick Be coatings (The Be will, in turn, have a thin coating of TiN to prevent multipactoring.) The alternating 2.8 T solenoidal field is produced with one solenoid per half cell, located between the RF cavities.

5. Heating in the absorbers

Heating of the LiH absorbers from the beam and RF fields need to be carefully understood. Melting or differential stresses could cause the thin beryllium layers to come off the LiH. The beam heating comes from dE/dx losses in the material. The maximum expected power deposited in the LiH is

$P_b = 10^{14}$ ppp x 2.5 Hz x 2 signs x 0.45 μ/p x 1.59 MeV/cm x 1 cm x 1.6 10^{-13} J/MeV
= 58 W

The power from the cylindrical pillbox RF cavity is deposited inside a skin depth of the beryllium layer facing the cavity. The expected RF power loss is

$$P_{rf} = \frac{\pi^2}{2}\frac{\delta}{\lambda}\frac{E_0^2 b^2}{Z_0}\left[J_1^2(\kappa) - J_0(\kappa)J_2(\kappa)\right]f_d$$

where δ is the skin depth, λ is the RF wavelength, E_0 is the peak RF electric field, b is the radius of the window, Z_0 is the impedance of free space, the J_i are Bessel functions and f_d is the pulse duty factor. The argument of the Bessel functions is

$$\kappa = x_{01}\frac{b}{a}$$

where x_{01} is the first zero of J_0 and a is the radius of the cavity. The skin depth δ of beryllium at 201.25 MHz is 8.6 μm, so all the RF power is confined to the inner Be layer. We have λ=1.5 m, E_0=15.25 MV/m, b=25 cm, a=59 cm, Z_0=377 Ω, x_{01}=2.405 and f_d=1.9 10^{-3}. This gives a total RF power loss of 220 W, which is four times the power deposited by the beam.

6. Channel performance

Figure 14 shows the variation of the transverse and longitudinal phase space along the front end. The solid curve shows the original conceptual design, while the dashed curve gives the more realistic simulation done for Study 2a.

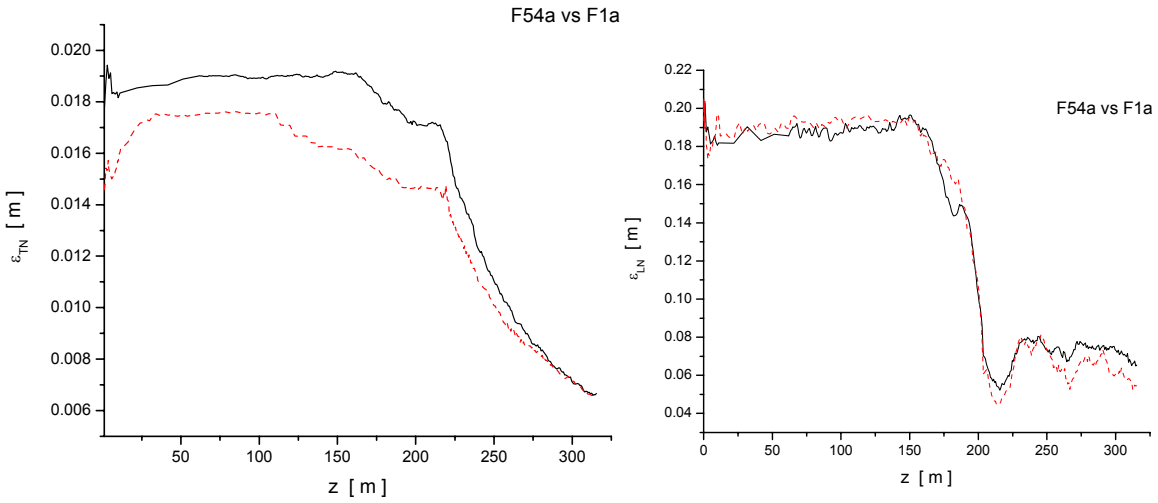

Figure 14. Normalized transverse (left) and longitudinal (right) emittance as a function of distance along the front end.

The cooling channel reduces the normalized transverse emittance by about a factor of 2. The change in longitudinal emittance comes from a cut that requires the data to lie in the momentum band 100 < p < 300 MeV/c. There is no longitudinal cooling in this channel.

The channel produces a final value of ϵ_{TN} = 7.1 mm rad. The equilibrium value for a LiH absorber with an 80 cm β function is about $\epsilon_{equil.T} \approx$ 5.5 mm rad.

Figure 15 shows the total muons per proton and the number of muons/proton that fit in the accelerator acceptance as a function of distance along the front end. The accelerator transverse normalized acceptance is A_T = 30 mm and normalized longitudinal acceptance is A_L = 150 mm.

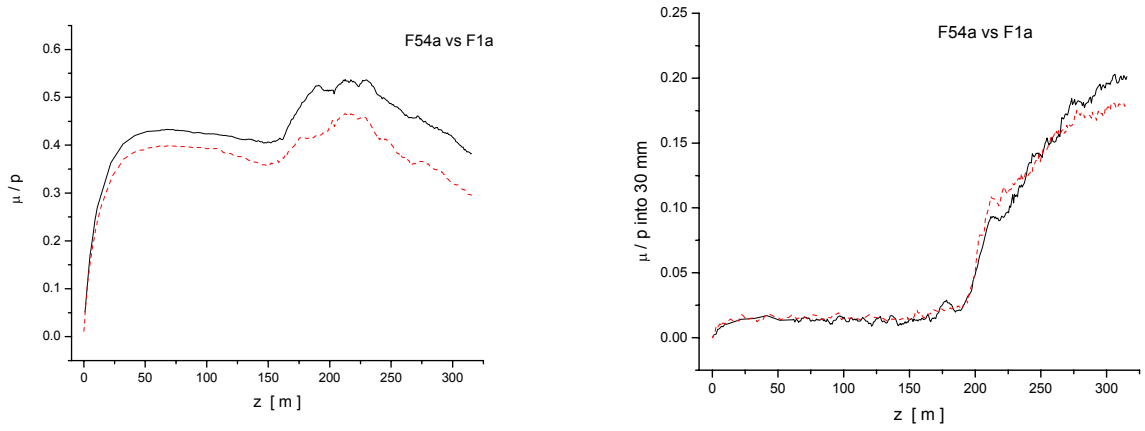

Figure 15. (left) Total muons/proton as a function of distance along the front end; (right) muons/proton inside the accelerator acceptance. Both distributions have a momentum selection 100 < p < 300 MeV/c.

The total number of muons in the momentum band falls by about 30% in the cooling channel. Decays account for 6%, while most of the remaining 24% are due to particles falling out of the full RF buckets. The 80-m-long cooling channel raises the muons/proton in the accelerator acceptance by about a factor of 1.7. The current best value for μ / p is 0.170±0.004. This is the same value obtained in FS2. Thus, we have achieved the identical performance at the entrance to the accelerator as FS2, but with a significantly simpler, shorter, and presumably less expensive channel design. The muons are distributed along a train of ~92 bunches at the end of the channel, as shown in Fig. 16.

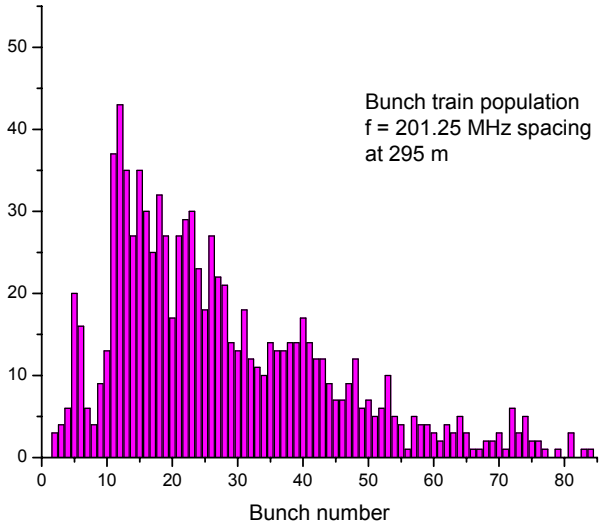

Figure 16. Muon bunch train population at the end of the channel.

The total transverse and longitudinal phase space occupied by the muon beam at the end of the channel is shown in Fig. 17.

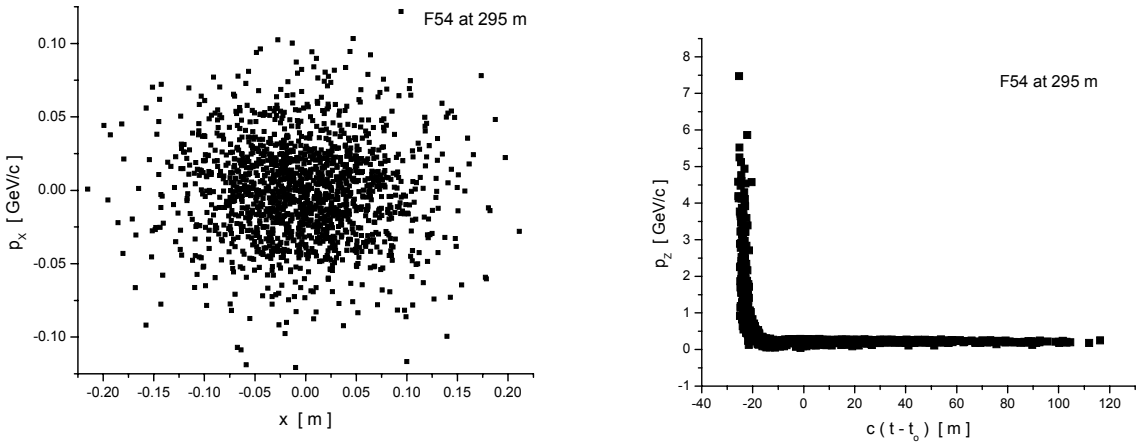

Figure 17. Total transverse (left) and longitudinal (right) phase space at the end of the channel.

The beam is mostly confined transversely inside a radius of 10 cm. Longitudinally the beam is divided into two parts. The useful part is spread out in time, but has a narrow energy spread. The other part of the beam, which is not useful, has a very large energy spread.

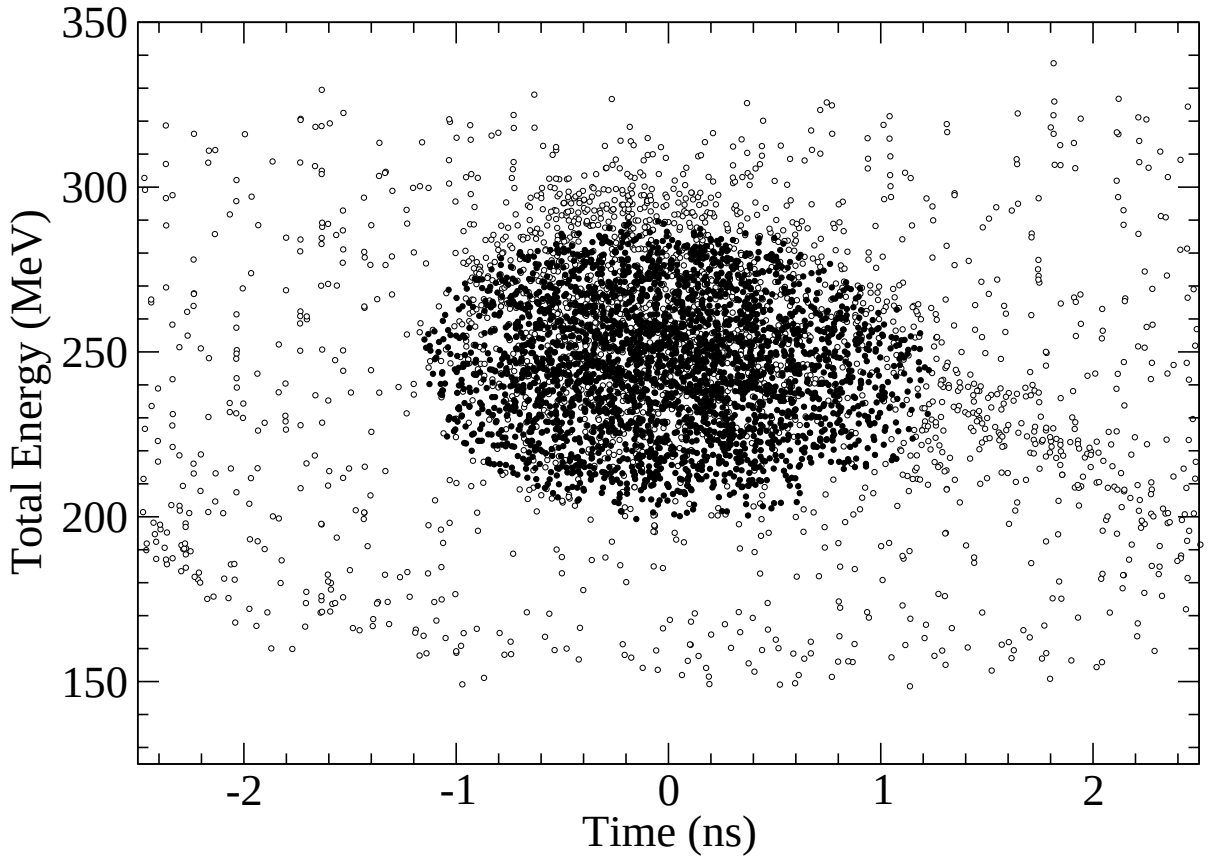

Figure 18. Longitudinal phase space of the overlapped bunches in the bunch train. The open circles are all particles that reach the end of the channel, while the filled circles are particles that lie within the accelerator acceptance.

The full 201 MHz RF bucket is clearly visible, along with the tail on the lower right of particles leaking out of the bucket.

In addition, unlike FS2, this channel transmits both signs of muons produced at the target. With appropriate modifications to the transport line going into the storage ring, this design could deliver both (time tagged) neutrinos and antineutrinos to the detector. Figure 19 shows a few interleaved μ^+ and μ^- bunches at the exit of the cooling section.

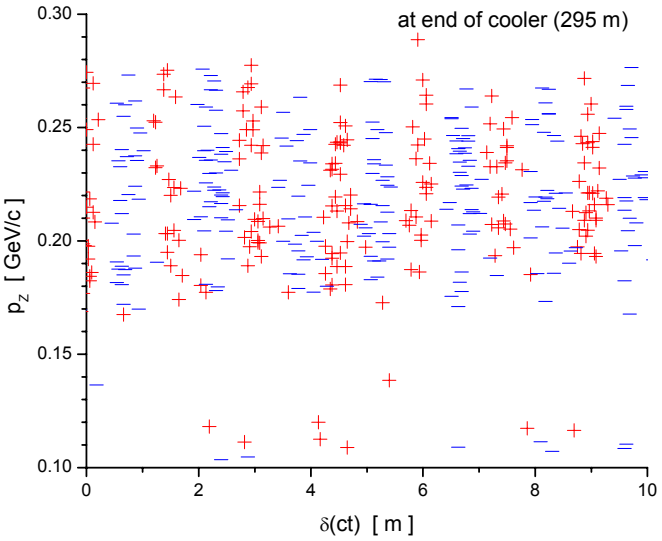

Figure 19. Part of the bunch train showing the interleaved positive (+) and negative (-) muon bunches.

7. Discussion

The front end design presented here gives a muon yield of $\mu / p = 0.17$ into the accelerator acceptance. This is the same yield given for Study 2, but with a simplified channel that is estimated to only cost about 53% of the Study 2 channel. In addition both signs of muons are transmitted through the channel, giving a potential gain in useful neutrino flux of a factor of 2. The design suffers in that there is no margin in the number of delivered muons. Many reasonable cost/benefit tradeoffs would cause the yield to drop below the neutrino factory requirements. We are still investigating possible modifications to increase the yield, but it may be ultimately necessary to give up some of the cost savings in order to do this. The other concern is the heating in the LiH absorbers. R&D will be necessary to see if the baseline design is acceptable. Fortunately we have several modified absorber designs that should have better thermal properties and which give only slightly worse muon yields.

Acknowledgements

We would like to thank Mike Zisman, John Cobb and Yasuo Fukui for useful discussions.

References

[1] S. Ozaki et al, Feasibility study II of a muon-based neutrino source, BNL report No. BNL-52623, June 2001.
[2] D. Neuffer, Exploration of the high-frequency buncher concept, MC note #269, February 2003.
[3] Study 2a web site, Neutrino Factory and Beta Beam Experiments and Development, BNL-72369, FNAL-TM-2259, LBNL-55478, 2004;
http://www.cap.bnl.gov/mumu/study2a/
[4] R. Palmer, Front end simulations, MC Meeting, Riverside, CA, January 2004,
http://www.cap.bnl.gov/mumu/conf/MC-040127/palmer-MC.pdf